On the Motion of a Sessile Drop on an Incline: Effect of Non-Monotonic Thermocapillary Stresses

On the Motion of a Sessile Drop on an Incline: Effect of Non-Monotonic Thermocapillary Stresses

Dimitrios Mamalis[1,a)] Vasileios Koutsos[1], Khellil Sefiane[1,2]

[1]Institute for Materials and Processes, School of Engineering, The University of Edinburgh, King's Buildings, Edinburgh EH9 3FB, United Kingdom

[2] Tianjin Key Lab of Refrigeration Technology, Tianjin University of Commerce, Tianjin City 300134, PR China

a) To whom correspondence should be addressed: E-mail: d.mamalis@ed.ac.uk

Abstract

We studied the short-time contact-line dynamics of a self-rewetting sessile droplet sliding ''freely'' on a silicone oil layer, on an inclined, uniformly heated substrate under non-isothermal conditions (liquid-solid). The effect of thermocapillarity and the contribution of surface tension gradients (Marangoni effect) to the droplet motion was investigated. The temperature of the substrate in conjunction with the non-monotonic surface tension/temperature dependence of the deformed self-rewetting droplet were found to significantly affect the early-stage inertial-capillary spreading regime. Infrared (IR) thermography images were also acquired to investigate the generation of thermal patterns at the liquid surface due to the strong surface-tension gradients. Our results demonstrate that the presence of strong surface tension driven flows at the liquid interface combined with droplet deformation (contact-angle hysteresis) give rise to complex droplet dynamics. The interplay between thermocapillary stresses and body forces result in enhanced spreading rates, temporal non-monotonic dependence of the contact-line speed as well as the droplet motion overcoming gravity in some instances.

Wetting and evaporation of a droplet deposited on a solid substrate are of importance to a large number of technological applications such as coatings, microfluidics and ink-jet printing technologies.[1–6] The interplay between the underlying mechanisms governing these phenomena is still under investigation and recognized as crucial in a wide range of biological, natural and industrial processes.[7–12] Droplet spreading and evaporation behavior is a complex phenomenon involving three phases, liquid-solid-vapor interactions through coupling by conduction with the substrate, convection/conduction within the drop and convection/diffusion in the vapor phase. When a droplet is deposited on a solid surface, it initially goes through a transient stage where the wetted contact line spreads until the liquid-solid-vapor system reaches its equilibrium state. The first stages of spreading tend to be rapid. The dynamics on how the drop reaches an equilibrium state varies depending on parameters including surface chemistry, liquid physicochemical properties and experimental conditions.[1,3,5]

Numerous studies have been conducted to understand the evolution of the internal liquid flows generated within a spreading and evaporating liquid drop, and the effect this has on wetting.[3,7,10,13–15] These characteristic flows within the drops are affected by liquid viscosity, surface tension, density, and the wettability of the substrate surface. In turn, internal flows affect the wetting behavior of liquids on solids. Moreover, adding thermal energy to the system (e.g. by a heated substrate) alters the temperature distribution inducing changes in the physical properties which complicate the phenomena and modify the wetting behavior of the droplet.

For the case of single-component droplets, a characteristic outward flow is induced, stemming from mass conservation to replenish liquid evaporating preferentially at the outer edge of the droplet.[7,16,17] During the evaporation of volatile liquid droplets, thermocapillary instabilities are developed when a system is subjected to sufficiently strong surface tension gradients. The origin of these fluid flow instabilities in volatile liquid droplets, is the thermocapillary effect which is driven by surface tension instabilities along the liquid interface due to temperature gradients.[10,13,14,18–21] The intensity and orientation of the Marangoni flow in a single-component system depend on the relative thermal properties of the substrate and the liquid, and the experimental conditions.[21–23] Surface-tension imbalances caused by temperature gradients along the liquid surface generate Marangoni flows which drive liquid from regions of low surface tension (hot) toward those of high surface tension (cold). On the other hand, for binary and generally multicomponent droplets the physical

behavior can be more complex. Previous studies with droplets formed by binary mixtures of water with alcohol (methanol,[24] ethanol,[25–29] butanol,[30,31] 1-propanol[32]) showed a different behavior as compared to those of pure liquids. The evaporation mechanism of these binary mixtures in particular involves three distinct stages: a first stage, where the more volatile component (alcohol) migrates to the liquid interface and evaporates first; a second stage which is transitional and involves evaporation of both components (mixed stage); and a last stage which mainly consists of the evaporation of the less volatile component of the mixture.[15,24,25,29] The present investigation is a study of binary alcohol droplets (dilute aqueous solutions of long-chain alcohols), namely self-rewetting fluids that have a non-monotonic (quasi-parabolic) dependence of the surface tension on temperature with a well-defined minimum, in a particular concentration range.[31,33–36] In such non-azeotropic solutions, the presence of Marangoni stresses are the result of temperature and/or concentration gradients namely thermocapillary and solutal effects, respectively. Interestingly, for higher temperatures beyond the temperature at which the minimum of the surface tension is observed, the reverse Marangoni effect occurs: these binary fluids spread i.e. 'self-rewet' by moving towards the warmer regions, thereby preventing dry-out of high temperature surfaces, thus improving the heat transfer performance of the systems.[33,37] Recent work carried out on self-rewetting fluids for space applications, demonstrated the importance of using these fluids revealing hence an increase in the efficiency e.g. heat transfer, of relevant devices such as heat pipes.[36,38]

The motion of liquid droplets on solids is relevant to a wide range of areas.[3,5] Body forces or external gradients can generate motion in liquid droplets.[39–41] Temperature differences between the liquid and substrate induce surface-tension gradient-driven droplet deformation and liquid flows from warmer to colder regions. Early experimental work by Bouasse[42] has shown that thermocapillarity can be the driving force for moving a drop upwards against gravity from the heated spot to the colder regions on a tilted wire. More recent studies involving horizontal and inclined substrates have shown that droplet motion is associated with the effect of contact-angle hysteresis and thermocapillary actuation.[43–48] These studies demonstrated the significant dependence of the contact angle on the induced surface-tension forces (Marangoni effect) and the deviation of the droplet's footprint from a circular shape.[43–48] Furthermore, wettability gradients induced by temperature gradients along a substrate have been found to influence the ensuing flows inside evaporating droplets.[40,41] Recently, Karapetsas *et al.* performed a full parametric finite-element study on the

thermocapillary motion of an inclined droplet with varying contact angles, focusing on the interplay between Marangoni stresses induced by thermocapillarity, gravity and contact-line dynamics. Their results have demonstrated that droplet motion is related to complex contact-line dynamics which included increased spreading rates and non-linear dependence of the contact-line speed on temperature.[48]

In the present letter, the migration of self-rewetting droplets on a heated inclined solid substrate coated with a silicone-oil layer, driven by thermocapillarity (Marangoni effect) against gravity was examined experimentally. We investigated a binary alcohol solution, consisting of water and 1-butanol (Sigma-Aldrich Co. LLC. 360465) 5% vol., on an inclined heated substrate. Experiments involved depositing ~3 μL to ~5 μL, droplets with a 10-fold repetition rate for each droplet volume on a ~5 degree inclined uniformly heated (~60±1 ^{o}C) borosilicate-glass substrate covered with silicon oil (~0.2 mm thickness). The silicon oil was employed in order to minimize the contact friction of the substrate. Binary-mixture temperatures were kept constant at 9±1 ^{o}C. A flexible heater SRGF-203/5-P-230V (OMEGALUX® Silicone Rubber Fiberglass Insulated Heaters) was placed underneath the substrate in order to uniformly heat the glass substrate. The substrate was a borosilicate-glass microscope coverslip with dimensions of: 24 mm × 50 mm × 100 μm from TAAB Laboratories Equipment Ltd., U.K. The experiments were conducted under controlled conditions i.e. relative humidity RH = 50 ± 5%, room temperature T = 21±1 ^{o}C and atmospheric pressure. The droplets rest on an oil coating and hence should not 'feel' the solid surface. This minimizes chemical inhomogeneities and substrate roughness effects, avoiding hence contact-line pinning behavior. Fig. 1 presents a sequence of images showing the motion of the sliding sessile droplet on the heated-glass slide coated with a silicon oil layer. Digital images of the spreading sessile droplets were recorded at 0.0167 s intervals and analyzed using the FTÅ200, Dynamic Contact Angle Analyzer, (First Ten Ångstroms, Inc., Portsmouth) software. Values for the droplet base radius r, height h, volume V, surface area A and contact angle θ were also extracted. It can be seen from the images in Fig. 1 that initially the sessile droplet slides and spreads (minimum contact friction on the silicone oil layer) due to the action of the gravitational force. Remarkably, at around t = 0.335 s the sliding-spreading droplet stops its downward movement and starts to climb the inclined heated substrate over a distance of few millimeters, against gravity, until t = 0.536 s, where the droplet stops moving.

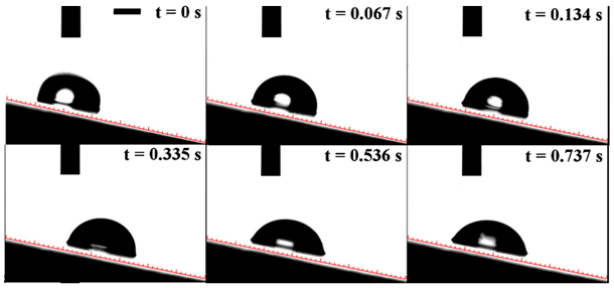

FIG. 1. Representative time sequence of images of a water –1-butanol 5% vol. sliding-spreading sessile droplet (~15 repetitions), volume ~4 μL, on an inclined (~5 degree) uniformly heated (60±1 ^{o}C) borosilicate glass substrate coated with a silicon oil layer (~ 0.2 mm thickness; layer applied before droplet deposition). The scale bar depicts a width of 1 mm, for all presented images.

Based on above findings, the spatiotemporal evolution of the droplet shape, the dynamics of the contact line, and droplet contact angles were analyzed. Fig. 2(a) depicts the evolution of the droplet advancing by θ_a and receding by θ_r contact angles versus time (see also image in Fig. 2(d)). The presence of contact-angle hysteresis of the droplet was clear and highlights the effect of droplet deformation during the sliding-spreading behavior. Fig. 2(b) presents the velocity U and base-diameter evolution of the sessile droplet on the inclined substrate over time, until the droplet arrives at a standstill (U = 0 mm/s). Moreover, the droplet dynamics of each side (2-d profile) i.e. velocity of the right edge (advancing θ_a) and left edge (receding θ_r) of the droplet were individually analyzed, Fig. 2(b). It is clear from the plotted evolution that the droplet's base diameter exhibited a slight spreading behavior during the initial downward motion, until t = 0.335 s where the droplet stopped and started to move upward against gravity. After a small oscillation period (~0.1 s) of the base diameter, the droplet spread significantly (during the upward motion) until t = 0.536 s (stationary position). The droplet continued to spread at the standstill until about t = 0.9 s, but with a clearly smaller spreading rate than previously i.e. slow viscous spreading dynamics. Fig. 2(c) depicts log-log plots of the contact-line dynamics $(r - r_o)$ versus time, showing that the spreading mechanism occurred in three characteristic stages having an $r - r_o \sim t^n$ dependency with spreading exponents n. We observed that at later times the droplets reached a stationary position but they continued to spread with characteristic low spreading rates (viscous-capillary regime) approximately following the well-known Tanner's law, $r \sim t^{0.1}$.[49] As time progressed, the temperature of the liquid phase became similar to the substrate's temperature, resulting finally in the complete evaporation of the liquid phase. It is worth noting that this

unusual droplet behavior occurred for advancing contact angles in the range of 90° to 101° ±1° and receding contact angles of between ca. 80° and 89° ±1° (after initial deposition of the sessile droplets on the inclined glass substrates treated with silicone oil). However, we observed enhanced spreading rates for all the experiments performed with the self-rewetting droplets due to the significant thermocapillary stresses (around the surface tension minimum region as a function of temperature) and the absence of contact-line friction forces, as presented in Fig. 2(c).

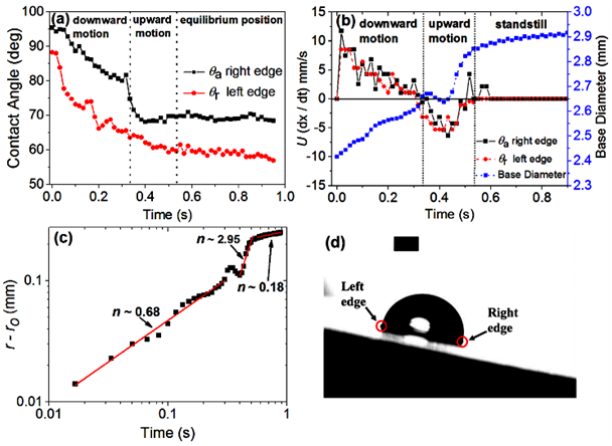

FIG. 2. Typical example (a) of the advancing θ_a and receding θ_r contact angles evolution (b) velocity of the two edges and base diameter profiles over time, of a water – 1-butanol 5% vol. sliding-spreading sessile droplet (~4 μL) on an inclined (~5 degree) uniformly heated (60±1 °C) borosilicate glass substrate coated with a silicon oil layer (around 0.2 mm thickness). (c) log-log plot measurements of the contact radius r (mm) plotted as a function of time (s) and the obtained spreading exponents n ($r - r_o \sim t^n$). (d) Image indicating the right and left edge of the droplet.

In order to assess the temperature distribution along the droplet surface, we have used infrared (IR) thermography on an inclined glass substrate (~5 degrees) to demonstrate the existence of Marangoni stresses (thermal patterns). The IR camera used in this study is an infrared (FLIR) ThermaCAM SC3000 that has a thermal sensitivity of 20 mK at 30 °C and an accuracy of 1% or 1 °C for temperatures up to 150 °C. The GaAs, Quantum Well Infrared Photon focal-plane array (FPA) detector has a spectral range of 8–9 μm of the infrared spectrum with a high resolution of 320 x 240 pixels. The images were recorded at 50 frames/s using a camera fitted with a microscope lens with 10 × 7.5 mm^2 field of view and a minimum focal length of 26 mm. Fig. 3 depicts the temperature profiles of the binary (water – 1-butanol

5% vol.) sessile droplets (9±1 ^{o}C) on an inclined glass substrate, at 60±1 ^{o}C. In Figs. 3(a)–3(d), the generation of characteristic thermal patterns (heat convection from the edges towards the center) at the interface of the binary alcohol droplets at t = ~0, ~0.33, ~0.53 and ~0.8 s, can be observed. This indicates that the droplet was in a transient phase with complex mixing flows, temperature gradients as well concentration differences between the two components (water and butanol). The generated thermal patterns were characterized by darker curved bands, with a preferential direction of propagation waves towards the droplet center. The development of these thermal patterns occurred spontaneously upon the deposition of the binary droplets on the heated substrate and they were organized radially and concentrically. Initially, the formation of the thermal patterns was more pronounced, Fig. 3(a), due to higher temperature differences between the droplet and the substrate. As time elapsed the intensity of the thermal patterns (and associated Marangoni stresses) became weaker and almost disappeared when the droplet reached a stationary position, Figs. 3(c) and 3(d), respectively. Fig. 3(e) presents the temperature distribution along the interface of the droplet at the four characteristic times. It can be seen from the temperature profiles in Fig. 3(e) that the center of the inclined droplet was slightly changed due to the presence of contact-angle hysteresis. The presence of the Marangoni effect along the liquid interface combined with contact-angle hysteresis gives rise to complex droplet behavior.

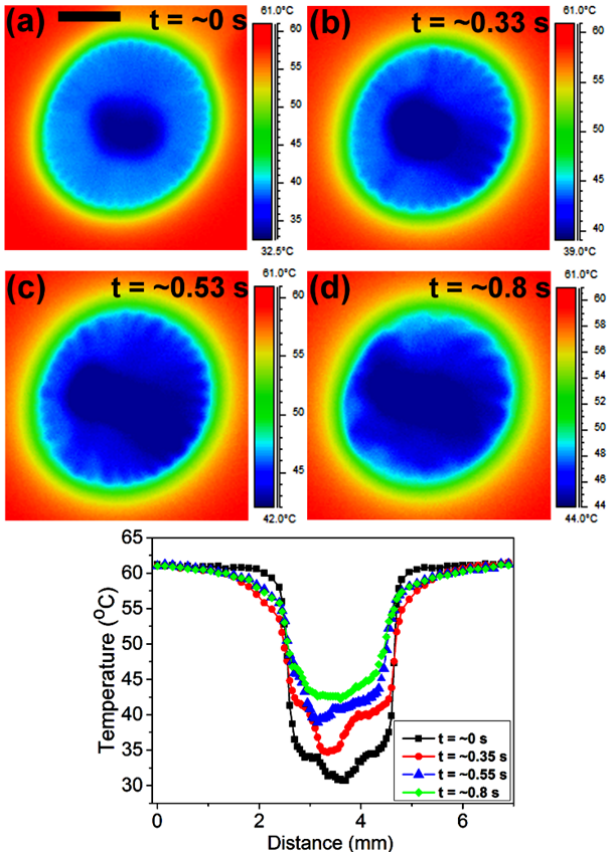

FIG. 3. (a)–(d): IR thermography visualization images of the temperature profile of sessile droplets (top view) of water – 1-butanol 5% vol. (volume of 4 ± 0.2 μL) on a uniformly heated inclined glass substrate (60±1 °C), (a) immediately after deposition (around 0 s), (b) ~0.33 s, (c) ~0.53 s and (d) ~0.8 s. The scale bar depicts a width of 1 mm, for all IR images. (e) four typical temperature profiles at t = ~0, 0.33, 0.53 and 0.8 s, respectively, along the surface of the evaporating inclined water-alcohol droplet.

The droplet motion was driven by gravity, capillarity, and Marangoni stresses arising from the dependence of surface tension on the temperature of the substrate. Immediately after contact, the droplet spread in both directions and concurrently the gravitational forces cause the downward movement of the sliding droplet on the silicone-oil layer. The temporal evolution of the wetted length and area changed the sliding-spreading droplet three-dimensional shape. The surface wettability can affect this behavior and even suppress it.[46–48,50–52]. In our case the droplet-shape changes are facilitated by the deposited oil layer which generates minimum contact-line friction. As the droplet slid and spread with different velocities (and contact angles), it deformed. It did this by adopting a contact-line area with a

corner regime at the rear side, from the initial round (spherical cap) shape (just after contact);[47,50,51] see Fig. 4(a): the red dot presents the droplet's center of mass and the blue vectors the surface-tension forces acting at the vicinity of the contact-line linked to wetted area changes; to draw this schematic we used WOLFRAM MATHEMATICA and MATLAB R2016a (MathWorks®) software. The droplet's center of mass is constantly changing position and thus irregularities in the body forces are expected to be present within the droplet during sliding. Temperature variations between the contact line (hot) and the apex (cold) of the sliding-spreading droplet gave rise to surface tension gradients (temperature and concentration) at the droplet interface resulting in Marangoni flows. Furthermore, the droplet deformation also generates non-uniform surface-tension gradient distribution between the two sides (right-left) of the contact line and the apex of the droplet, as presented in Fig. 4(b).

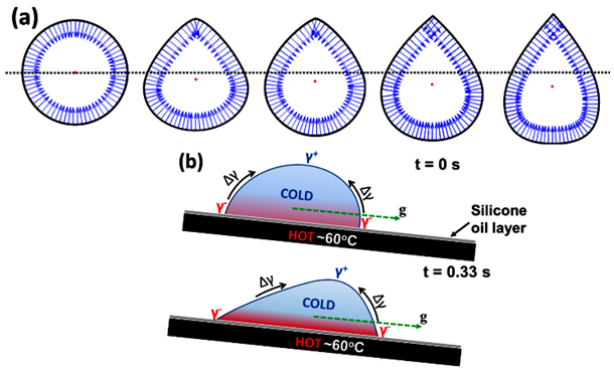

FIG. 4. (a) Schematic drawing of the droplet deformation during sliding-spreading behavior where red dots present the droplet's center of mass and blue vectors the surface tension forces acting at the contact line (b) schematic presentation of the surface tension gradients (Marangoni effect) presented at the interface of the self-rewetting droplet on the inclined substrate at t = ~0 s and ~0.33 s, respectively.

The surface tension of the self-rewetting fluid (water – 1-butanol 5% vol.) has been measured in the temperature range from ~10 to ~90 ^{o}C, using the pendant drop method analysis (FTÅ apparatus), Fig. 5(a). The quasi-parabolic dependence of the self-rewetting surface tension on temperature is clear. The minimum of the surface tension was measured to be around 63 ^{o}C and the non-monotonic temperature dependence for these fluids was revealed. At t = ~0 s, Fig. 5(b), the surface tension difference at the left side ($\theta_r = 87^o$) of the contact line (warm)

and the droplet apex (cold) was calculated to be roughly: $\Delta\gamma_{LEFT} \approx 0.09\frac{\mathrm{mN}}{\mathrm{m}}$ and at the right side ($\theta_a = 95^o$) was: $\Delta\gamma_{RIGHT} \approx 0.13\frac{\mathrm{mN}}{\mathrm{m}}$. The gravity (strong effect) and the Marangoni stresses (weak effect) are acting in the same direction, enhancing the downward motion of the self-rewetting droplet. Interestingly, at *t* = ~0.33 s, just before the droplet started the upward motion, the calculated overall surface-tension differences between the contact line and the droplet apex for the two sides of the droplet were: $\Delta\gamma_{LEFT} \approx 0.25\frac{\mathrm{mN}}{\mathrm{m}}$ ($\theta_r = 65^o$), and $\Delta\gamma_{RIGHT} \approx -0.40\frac{\mathrm{mN}}{\mathrm{m}}$ ($\theta_a = 74^o$), respectively, Fig. 5(c). The deformed droplet's motion was influenced by gravity and the presence of strong Marangoni stresses, but were acting in the opposite direction than at *t* = ~0 s (Fig 5(a)). That is to say, at the right side (edge) of the droplet, the surface-tension difference was higher than on the left side and of opposite sign (direction), resulting in the upward movement against gravity. At *t* = ~0.53 s when the droplet stopped the upward motion (but continued the spreading behavior) the calculated surface tension differences along the interface were roughly: $\Delta\gamma_{LEFT} \approx 0.19\frac{\mathrm{mN}}{\mathrm{m}}$ ($\theta_r = 62^o$) and $\Delta\gamma_{RIGHT} \approx -0.21\frac{\mathrm{mN}}{\mathrm{m}}$ ($\theta_a = 69^o$) at the left and right sides of the droplet, respectively, Fig 5(d). The surface tension stresses between the two sides of the droplet (advancing and receding) at *t* = ~0.53 s, were more balanced as compared at *t* = ~0.33 s and were clearly associated with the decreasing thermal pattern activity (Marangoni effect), Fig 3(c), and with the droplet's stagnation point. Another clear feature revealed, from this series of experiments, in the absence of contact line friction forces (silicone oil) and the presence of strong Marangoni stresses (surface-tension-temperature-concentration gradients), was the drastically enhanced spreading rates of the self-rewetting droplets, Fig. 2(c).

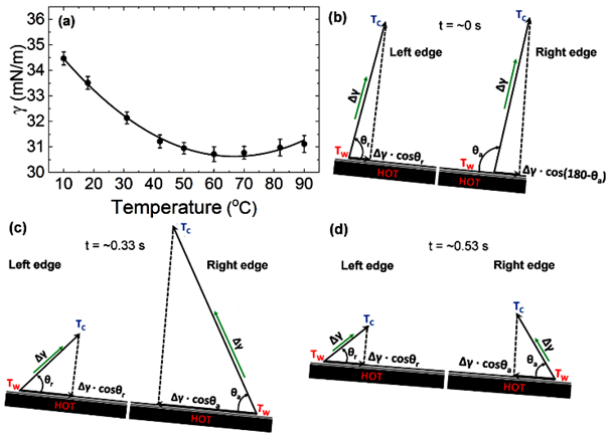

FIG. 5. (a) Surface tension measurements (mN/m) of the self-rewetting fluids: water – 1-butanol 5% vol., in the temperature range from 10 – 90 ^{o}C, under controlled experimental conditions. Schematic drawing of the surface tension forces acting at the vicinity of the contact line of the self-rewetting droplet at two different times: (b) t = ~0 s (immediately after contact), (c) t = ~0.33 s (when the droplet started the upward motion) and (d) t = ~0.53 s (the sliding-movement of the droplet stopped but continued wetting with lower rate).

In summary, it was observed that the inclination of the surface which caused the droplet deformation combined with the presence of strong thermocapillary stresses and gravity played a significant role in the droplet's complicated contact-line dynamics. The observation of characteristic thermal patterns at the surface of the evaporating droplets indicates the existence of thermocapillary/solutal effects resulting in internal flows. The interplay between Marangoni stresses induced by surface-tension-driven flows and droplet deformation caused the contact line to move in opposite directions against gravity. Understanding the underlying physical mechanisms affecting wetting phenomena can provide the means to control fluid motion in an unprecedented manner which can play a key role in many applications.

This work was carried out under the umbrella of COST ActionMP1106: "Smart and green interfaces – from single bubbles and drops to industrial, environmental and biomedical applications". We acknowledge funding from the Engineering and Physical Sciences Council (EPSRC) DTA.

References

[1] P.G. de Gennes, Rev. Mod. Phys. **57**, 827 (1985).

[2] P.G. Simpkins and V.J. Kuck, J. Colloid Interface Sci. **263**, 562 (2003).

[3] P.G. de Gennes, F. Brochard-Wyart, and D. Quere, *Capillarity and Wetting Phenomena: Drops, Bubbles, Pearls, Waves* (Springer New York, 2003).

[4] P. Tabeling, Comptes Rendus Phys. **5**, 519 (2004).

[5] D. Bonn, J. Eggers, J. Indekeu, J. Meunier, and E. Rolley, Rev. Mod. Phys. **81**, 739 (2009).

[6] M. Singh, H.M. Haverinen, P. Dhagat, and G.E. Jabbour, Adv. Mater. **22**, 673 (2010).

[7] R.D. Deegan, O. Bakajin, T.F. Dupont, G. Huber, S.R. Nagel, and T.A. Witten, Nature **389**, 827

(1997).

[8] H. Hu and R.G. Larson, J. Phys. Chem. B **106**, 1334 (2002).

[9] H.Y. Erbil, G. McHale, and M.I. Newton, Langmuir **18**, 2636 (2002).

[10] H. Hu and R.G. Larson, Langmuir **21**, 3972 (2005).

[11] K. Sefiane, S.K. Wilson, S. David, G.J. Dunn, and B.R. Duffy, Phys. Fluids **21**, 62101 (2009).

[12] H.Y. Erbil, Adv. Colloid Interface Sci. **170**, 67 (2012).

[13] M.J. Block, Nature **178**, 650 (1956).

[14] H. Hu and R.G. Larson, Langmuir **21**, 3963 (2005).

[15] R. Bennacer and K. Sefiane, J. Fluid Mech. **749**, 649 (2014).

[16] R.D. Deegan, Phys. Rev. E **61**, 475 (2000).

[17] R.D. Deegan, O. Bakajin, T.F. Dupont, G. Huber, S.R. Nagel, and T.A. Witten, Phys. Rev. E **62**, 756 (2000).

[18] H. Bénard, J. Phys. Theor. Appl. **10**, 254 (1901).

[19] J.R.A. Pearson, J. Fluid Mech. **4**, 489 (2006).

[20] L.E. Scriven and C. V Sternling, J. Fluid Mech. **19**, 321 (2006).

[21] H. Ghasemi and C.A. Ward, Phys. Rev. Lett. **105**, 136102 (2010).

[22] H. Hu and R.G. Larson, J. Phys. Chem. B **110**, 7090 (2006).

[23] W.D. Ristenpart, P.G. Kim, C. Domingues, J. Wan, and H.A. Stone, Phys. Rev. Lett. **99**, 234502 (2007).

[24] K. Sefiane, S. David, and M.E.R. Shanahan, J. Phys. Chem. B **112**, 11317 (2008).

[25] K. Sefiane, L. Tadrist, and M. Douglas, Int. J. Heat Mass Transf. **46**, 4527 (2003).

[26] A.K.H. Cheng, D.M. Soolaman, and H.Z. Yu, J. Phys. Chem. B **110**, 11267 (2006).

[27] L. Shi, P. Shen, D. Zhang, Q. Lin, and Q. Jiang, Surf. Interface Anal. **41**, 951 (2009).

[28] C. Liu and E. Bonaccurso, Rev. Sci. Instrum. **81**, 13702 (2010).

[29] Y. Hamamoto, J.R.E. Christy, and K. Sefiane, J. Therm. Sci. Technol. **7**, 425 (2012).

[30] R. Savino, N. di Francescantonio, R. Fortezza, and Y. Abe, Acta Astronaut. **61**, 16 (2007).

[31] R. Savino, A. Cecere, and R.D. Paola, Int. J. Heat Fluid Flow **30**, 380 (2009).

[32] S.M. Rowan, M.I. Newton, F.W. Driewer, and G. McHale, J. Phys. Chem. B **104**, 8217 (2000).

[33] R. Vochten and G. Petre, J. Colloid Interface Sci. **42**, 320 (1973).

[34] M.C. Limbourg, J.C. Legros, and G. Petre, Adv. Sp. Res. **6**, 35 (1986).

[35] G. Petre and M.A. Azouni, J. Colloid Interface Sci. **98**, 261 (1984).

[36] R. Savino, A. Cecere, S. Van Vaerenbergh, Y. Abe, G. Pizzirusso, W. Tzevelecos, M. Mojahed, and Q. Galand, Acta Astronaut. **89**, 179 (2013).

[37] Y. Abe, A. Iwasaki, and K. Tanaka, Ann. N.Y. Acad. Sci. **1027**, 269 (2004).

[38] Y. Hu, T. Liu, X. Li, and S. Wang, Int. J. Heat Mass Transf. **70**, 496 (2014).

[39] F. Brochard, Langmuir **5**, 432 (1989).

[40] S. Daniel, M.K. Chaudhury, and J.C. Chen, Science (80-.). **291**, 633 (2001).

[41] D.T. Wasan, A.D. Nikolov, and H. Brenner, Science (80-.). **291**, 605 (2001).

[42] H. Bouasse, *Capillarité phénomènes superficiels* (Delagrave, Paris, 1924).

[43] V. Pratap, N. Moumen, and R.S. Subramanian, Langmuir **24**, 5185 (2008).

[44] J.Z. Chen, S.M. Troian, A.A. Darhuber, and S. Wagner, J. Appl. Phys. **97**, 14906 (2005).

[45] J.M. Gomba and G.M. Homsy, J. Fluid Mech. **647**, 125 (2010).

[46] G. Karapetsas, K.C. Sahu, and O.K. Matar, Langmuir **29**, 8892 (2013).

[47] B.A. Puthenveettil, V.K. Senthilkumar, and E.J. Hopfinger, J. Fluid Mech. **726**, 26 (2013).

[48] G. Karapetsas, K.C. Sahu, K. Sefiane, and O.K. Matar, Langmuir **30**, 4310 (2014).

[49] L.H. Tanner, J. Phys. D-Applied Phys. **12**, 1473 (1979).

[50] P. Brunet, J. Eggers, and R.D. Deegan, Eur. Phys. J. Spec. Top. **166**, 11 (2009).

[51] P. Sartori, D. Quagliati, S. Varagnolo, M. Pierno, G. Mistura, F. Magaletti, and C.M. Casciola, New J. Phys. **17**, 113017 (2015).

[52] M. Musterd, V. van Steijn, C.R. Kleijn, and M.T. Kreutzer, Phys. Rev. Lett. **113**, 66104 (2014).

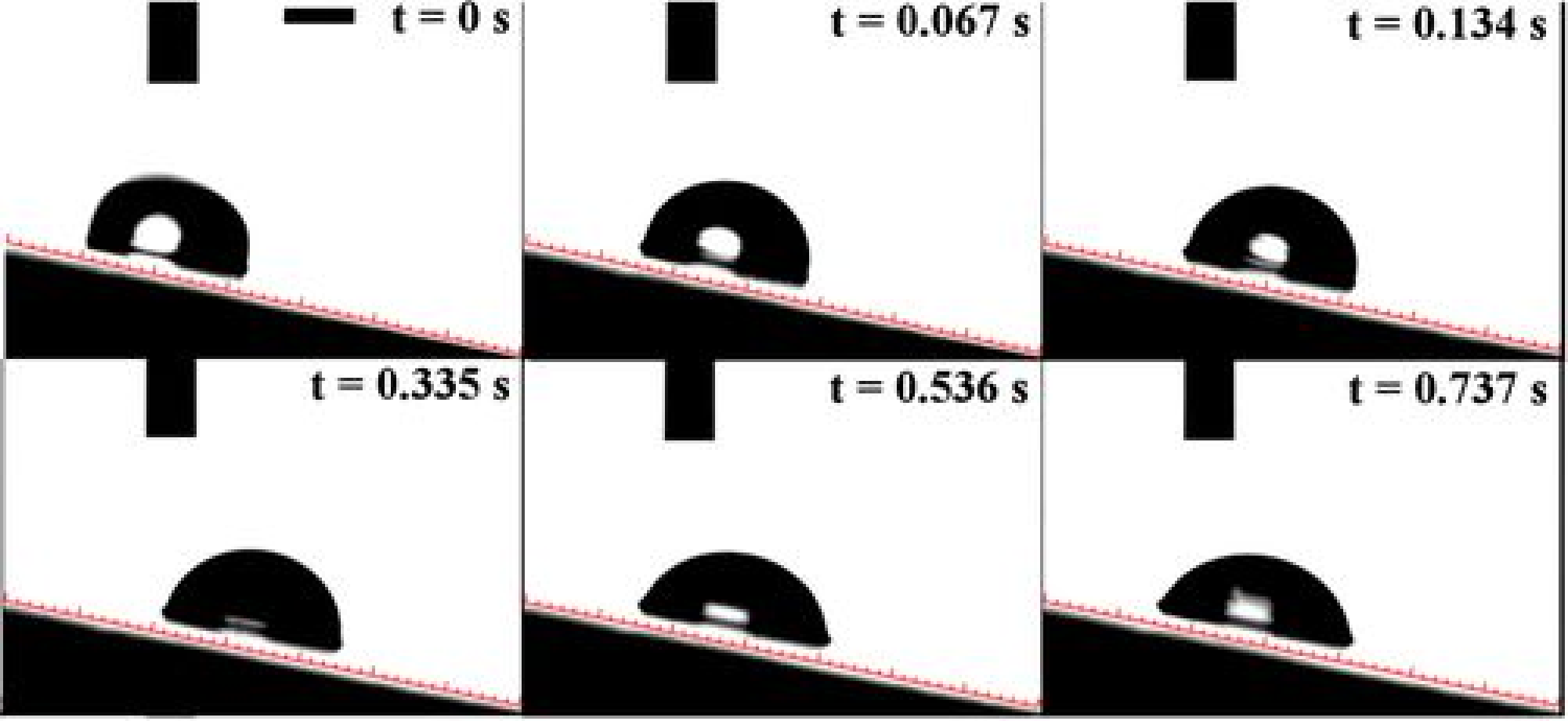
t = 0 s
t = 0.067 s
t = 0.134 s
t = 0.335 s
t = 0.536 s
t = 0.737 s

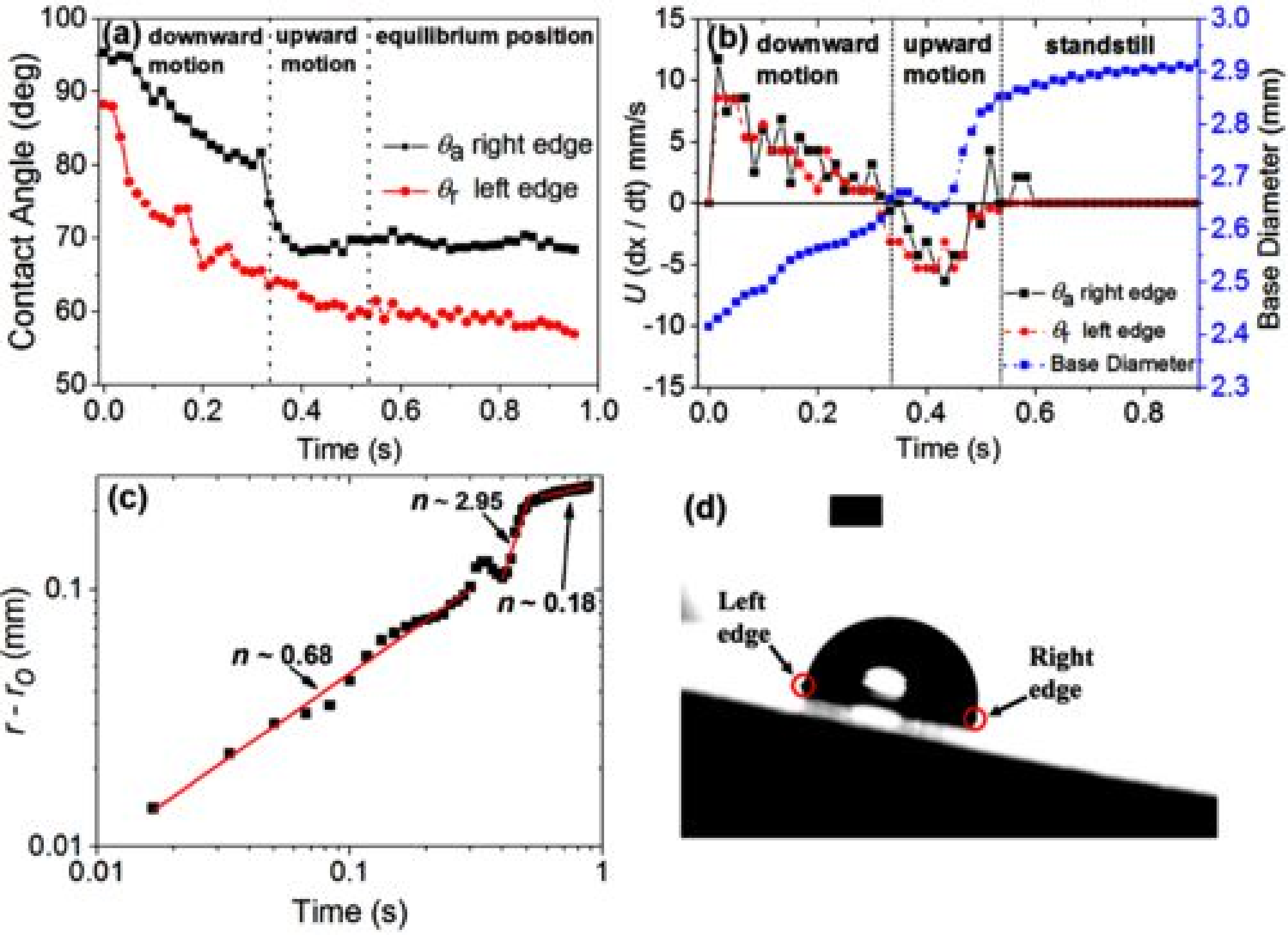
(a)
downward motion
upward motion
equilibrium position
Contact Angle (deg)
Time (s)
θa right edge
θf left edge
(b)
downward motion
upward motion
standstill
U (dx / dt) mm/s
Base Diameter (mm)
Time (s)
θa right edge
θf left edge
Base Diameter
(c)
n ~ 2.95
n ~ 0.18
n ~ 0.68
r - r0 (mm)
Time (s)
(d)
Left edge
Right edge

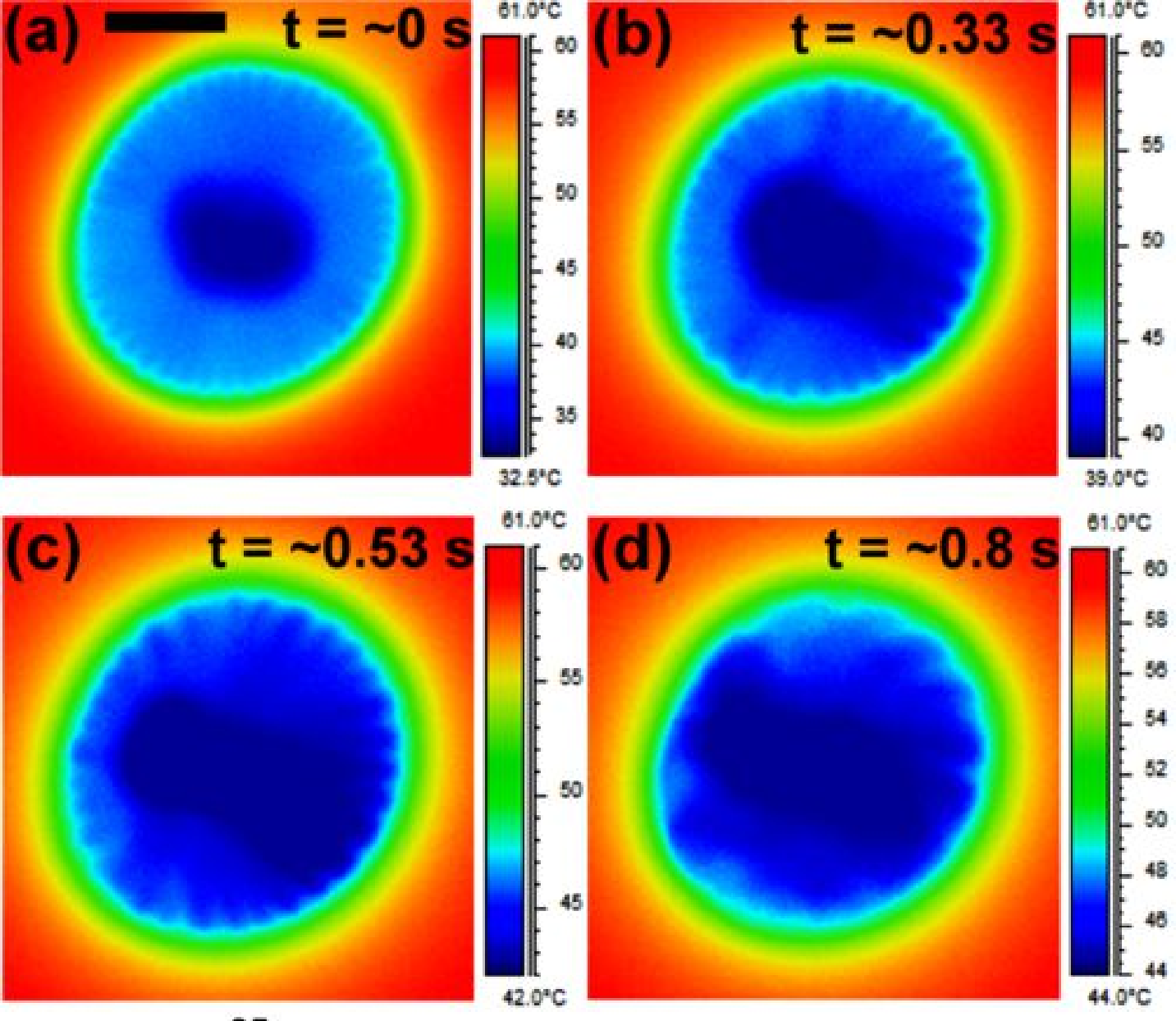
(a)
t = ~0 s
61.0°C
60
55
50
45
40
35
32.5°C
(b)
t = ~0.33 s
61.0°C
60
55
50
45
40
39.0°C
(c)
t = ~0.53 s
61.0°C
60
55
50
45
42.0°C
(d)
t = ~0.8 s
61.0°C
60
58
56
54
52
50
48
46
44
44.0°C

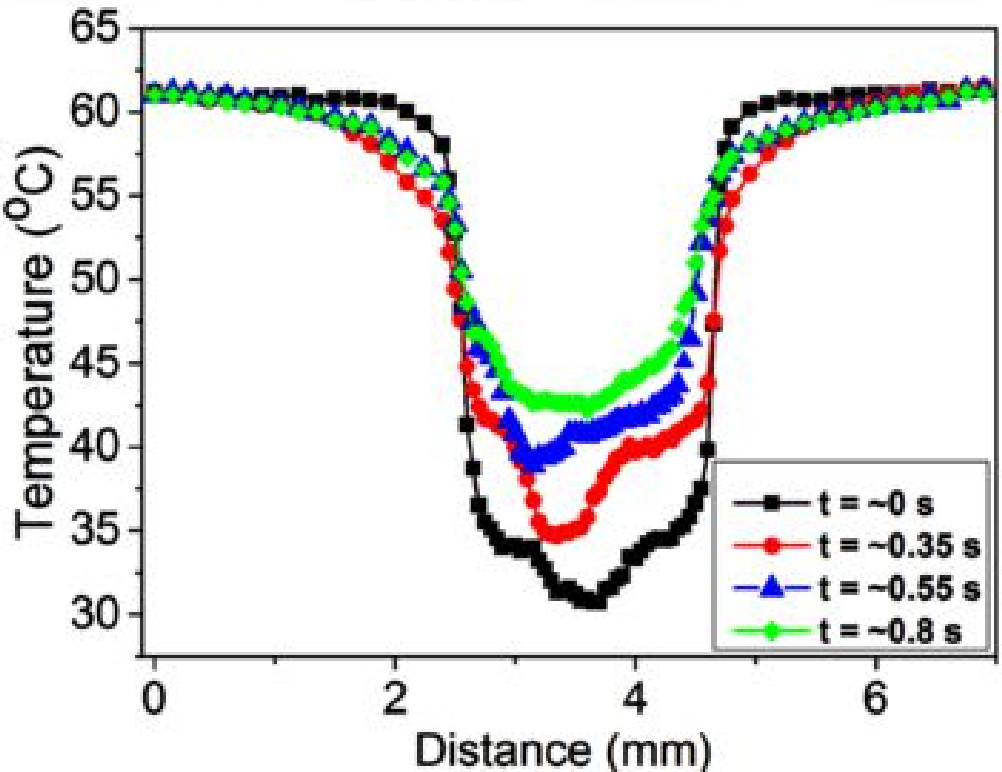
Temperature (°C)
65
60
55
50
45
40
35
30
0
2
4
6
Distance (mm)
t = ~0 s
t = ~0.35 s
t = ~0.55 s
t = ~0.8 s

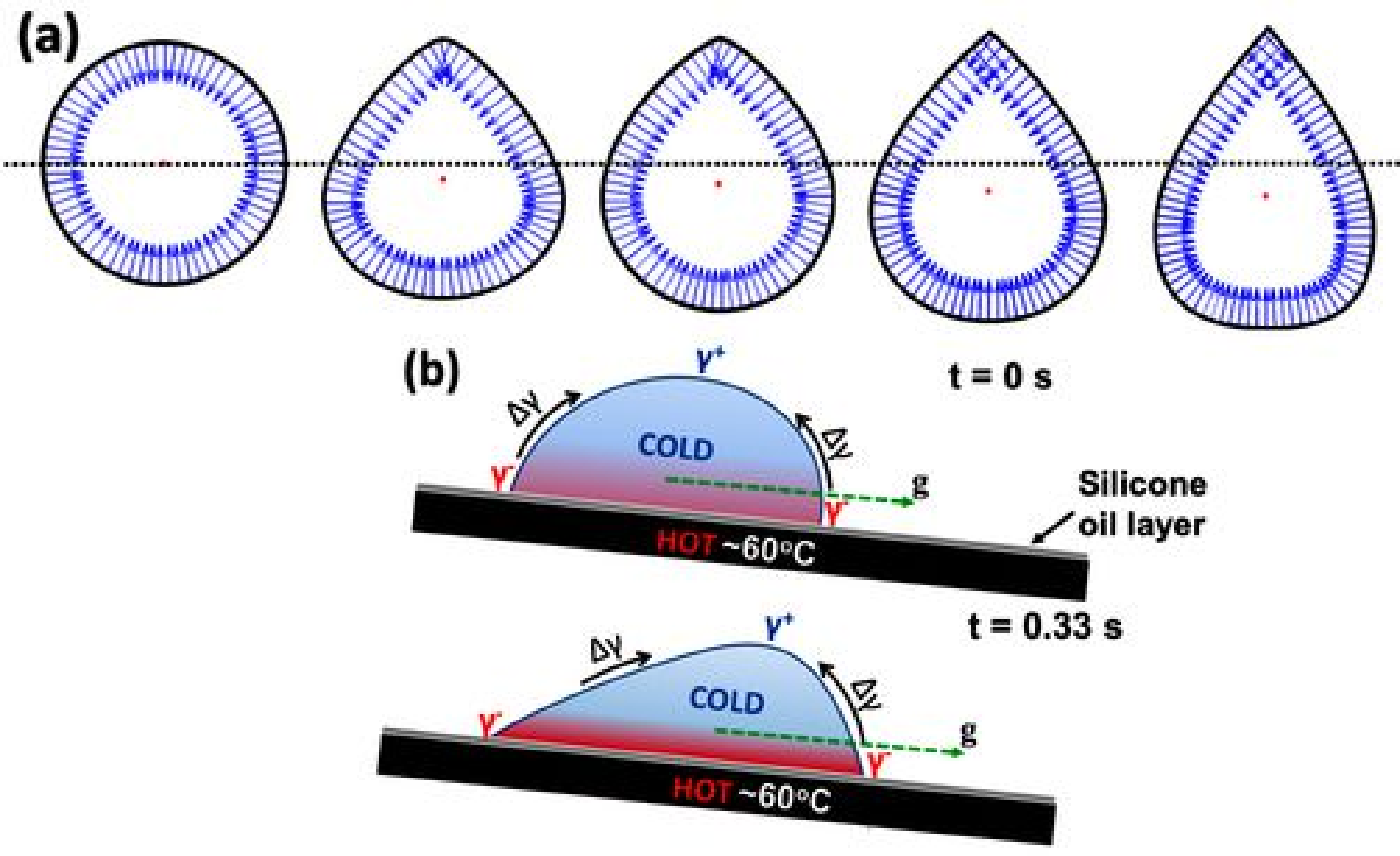
(a)
(b)
t = 0 s
γ+
Δγ
Δγ
γ-
COLD
g
Silicone
oil layer
HOT ~60°C
t = 0.33 s
γ+
Δγ
Δγ
γ-
COLD
g
HOT ~60°C

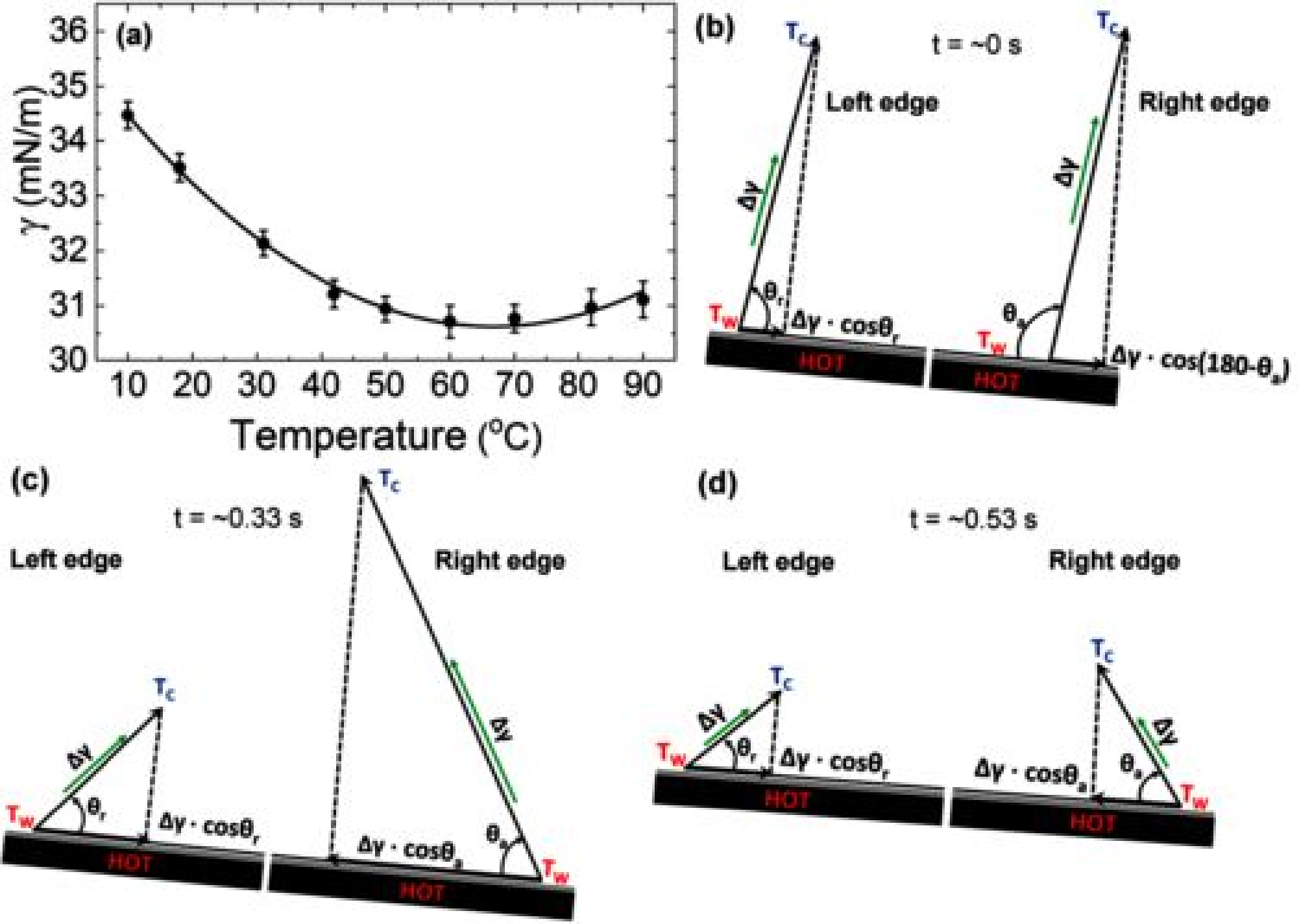
(a)
γ (mN/m)
36
35
34
33
32
31
30
10 20 30 40 50 60 70 80 90
Temperature (°C)
(b)
t = ~0 s
Left edge
Right edge
T_C
T_W
Δγ
$θ_r$
$θ_a$
Δγ · cosθ$_r$
Δγ · cos(180-θ$_a$)
HOT
(c)
t = ~0.33 s
Left edge
Right edge
(d)
t = ~0.53 s
Left edge
Right edge